Supporting Information for

Crystalline MoS$_2$ enhanced conductive black titania for efficient solar to chemical conversions: photocatalytic CO$_2$ reduction and CH$_4$ oxidation

Qingyuan Bi,*[ab] Min Wang,[b] Muhammad Sohail Riaz,[c] Xianlong Du,[d] Guisheng Li[a] and Fuqiang Huang*[be]

[a] School of Materials and Chemistry, University of Shanghai for Science and Technology, Shanghai 200093, P. R. China

[b] State Key Laboratory of High Performance Ceramics and Superfine Microstructure, Shanghai Institute of Ceramics, Chinese Academy of Sciences, Shanghai 200050, P. R. China

[c] School of Materials Science and Engineering, Gwangju Institute of Science and Technology, Gwangju 61005, Republic of Korea

[d] Key Laboratory of Interfacial Physics and Technology, Shanghai Institute of Applied Physics, Chinese Academy of Sciences, Shanghai 201800, P. R. China

[e] State Key Laboratory of Rare Earth Materials Chemistry and Applications, College of Chemistry and Molecular Engineering, Peking University, Beijing 100871, P. R. China

* Corresponding Authors
Email: qybi@usst.edu.cn; huangfq@mail.sic.ac.cn

1. Catalyst characterization

BET-specific surface areas of the prepared catalysts were determined by adsorption–desorption of N_2 at liquid nitrogen temperature using the Micromeritics ASAP 2460 equipment. Sample degassing was carried out at 300 °C before acquiring the adsorption isotherm.

X-ray diffraction (XRD) analysis was carried out on a Bruker D8 Advance X-ray diffractometer applying the Ni-filtered Cu Kα radiation at 40 kV and 40 mA.

X-ray photoelectron spectroscopy (XPS) data were recorded with the Axis Ultra Photoelectron Spectrometer through a monochromatized Al Kα anode (225 W, 15 kV, 15 mA). The C 1s peak located at 284.8 eV was employed as the reference for calibrating the binding energies (BE).

Raman spectra were recorded in a Thermal Dispersive Spectrometer applying a 10 mW laser with an excitation wavelength of 532 nm.

Ultraviolet-visible (UV-Vis) spectra were recorded on a Hitachi U4100 Spectrometer equipped with the integrating sphere and reference $BaSO_4$. The solar absorption was obtained by the following equation (S1):

$$A = \frac{\int (1-T) \cdot S \cdot d\lambda}{\int S \cdot d\lambda} \tag{S1}$$

Where A is the solar absorption, λ is the wavelength (nm), T is the reflectance, S is the light spectral irradiance (W m^{-2} nm^{-1}), and $(1-T) \cdot S$ is the catalyst absorption of solar spectral irradiance.

Photoluminescence (PL) spectra were conducted at 320 nm using a MODEL Fluoro Max-3 fluorescence spectrophotometer at room temperature.

The photothermic effect was performed on a thermal infrared imager SC305 by irradiating an AM 1.5G Xe lamp solar simulator.

A JEOL 2011 microscope conducted at 200 kV coupled with an EDX unit (Si(Li) detector) was employed for the transmission electron microscopy (TEM) analysis.

A JEM 2100F electron microscope working at 200 kV coupled with an EDX unit (Si(Li) detector) was conducted for the high-resolution TEM (HRTEM) analysis.

CH_4 adsorption was measured by temperature-programmed desorption of CH_4 (CH_4-TPD) experiments using

AutoChem HP 2950 apparatus. Typically, the catalyst (0.2 g) was pretreated at 200 °C for 2 h and then cooled to 50 °C in flowing Ar. Later, CH_4 gas was introduced until adsorption saturation (0.5 h), followed by purging with Ar flow (30 mL min^{-1}) for 1 h. Subsequently, the temperature was raised from 50 to 600 °C (5 °C min^{-1}) to desorb CH_4. The desorbed CH_4 gas was determined by on-line gas chromatography (GC) with a thermal conductivity detector (TCD).

2. Solar to chemical energy conversion

Photocatalytic CO_2 reduction: The experiments were carried out in a high-pressure stainless autoclave reactor (100 mL) with a reflux condenser and a quartz window on the top. The solar light irradiation was from a 300 W Xe lamp (Aulight CEL-HX, Beijing), and the light power was calibrated to AM 1.5 by an NREL-calibrated Si cell (Oriel 91150). The visible light was attained using a light reflector of 400~780 nm, and the reflectivity was greater than 95%. Typically, 6 mL of deionized water was first added to the reactor. Then, a 50 mg sample was ultrasonically dispersed in 0.5 mL deionized water and drop-dried on a clean glass sheet, placing the holder in the vessel's upper region. Later, the autoclave was sealed, and the internal air gas was degassed completely using high-purity CO_2 twenty times at ambient temperature, and then 2 bar CO_2 gas was charged. The stirrer was started (800 rpm) when the light was irradiated. After a particular reaction, the reactor was placed into the cool water, and the inside gas was collected carefully. An Agilent 7820A GC analyzed the gaseous mixture and liquid product with a capillary column (HP-5) connected to an FID or a packed column (TDX-01) connected to a TCD. The electron-transferred CH_4 selectivity was calculated according to the following equation (S6):

$$H_2O + 2h^+ \rightarrow 1/2O_2 + 2H^+ \tag{S2}$$

$$CO_2 + 8H^+ + 8e^- \rightarrow CH_4 + 2H_2O \tag{S3}$$

$$CO_2 + 2H^+ + 2e^- \rightarrow CO + H_2O \tag{S4}$$

$$2H^+ + 2e^- \rightarrow 2H_2 \tag{S5}$$

$$CH_4 \text{ selectivity (\%)} = 8n(CH_4)/[8n(CH_4) + 2n(CO) + 2n(H_2)] \times 100\% \tag{S6}$$

Where $n(CH_4)$, $n(CO)$, and $n(H_2)$ represent the moles of produced CH_4, CO, and H_2, note that three separate tests were carried out for each test. The stability was conducted on a 50 mg catalyst condition, 6 mL H_2O, 2 bar CO_2, and solar light irradiation for a continuous 5 h in each run. The used sample was washed with deionized water several times and dried overnight for reuse.

The STYs of CH_4, CO, and H_2 were calculated according to the following equations (S7–S9):

$$\text{STY of CH}_4 = \frac{\text{Amount of CH}_4 \text{ (μmol)}}{\text{Catalyst amount (g)} \times \text{Reaction time (h)}} \qquad \text{(S7)}$$

$$\text{STY of CO} = \frac{\text{Amount of CO (μmol)}}{\text{Catalyst amount (g)} \times \text{Reaction time (h)}} \qquad \text{(S8)}$$

$$\text{STY of H}_2 = \frac{\text{Amount of H}_2 \text{ (μmol)}}{\text{Catalyst amount (g)} \times \text{Reaction time (h)}} \qquad \text{(S9)}$$

Photocatalytic CH$_4$ oxidation: The reactions were conducted in a high-pressure stainless autoclave (50 mL) with a condenser and a quartz window on the top. Typically, 9 mL deionized water, 1 mL 30% H$_2$O$_2$, and 50 mg catalyst were placed in the reactor. The autoclave was sealed and degassed several times with 5 bar CH$_4$ to remove the internal air, then 20 bar CH$_4$ was charged. The stirrer (800 rpm) was started when the light was irradiated. The reactor's temperature was kept at room temperature. After a particular time, the reactor was placed in cool water, and the inside gas was collected carefully. The liquid mixture was transferred into a centrifuge tube, and the solid catalyst was separated by centrifugation. An Agilent 7820A GC analyzed both gaseous mixture and liquid product. Identification of the products was conducted using a GC-MS spectrometer (Shimadzu GCMS-QP2010 SE). Note that the total carbon balance of >95% was achieved, and three separate tests were carried out for each test. The centrifuged samples from parallel tests were collected, washed, and dried for reuse for the recycling reaction.

The STYs of methanol and ethanol were calculated according to the following equations (S10 and S11):

$$\text{STY of methanol} = \frac{\text{Amount of methanol (μmol)}}{\text{Catalyst amount (g)} \times \text{Reaction time (h)}} \qquad \text{(S10)}$$

$$\text{STY of ethanol} = \frac{\text{Amount of ethanol (μmol)}}{\text{Catalyst amount (g)} \times \text{Reaction time (h)}} \qquad \text{(S11)}$$
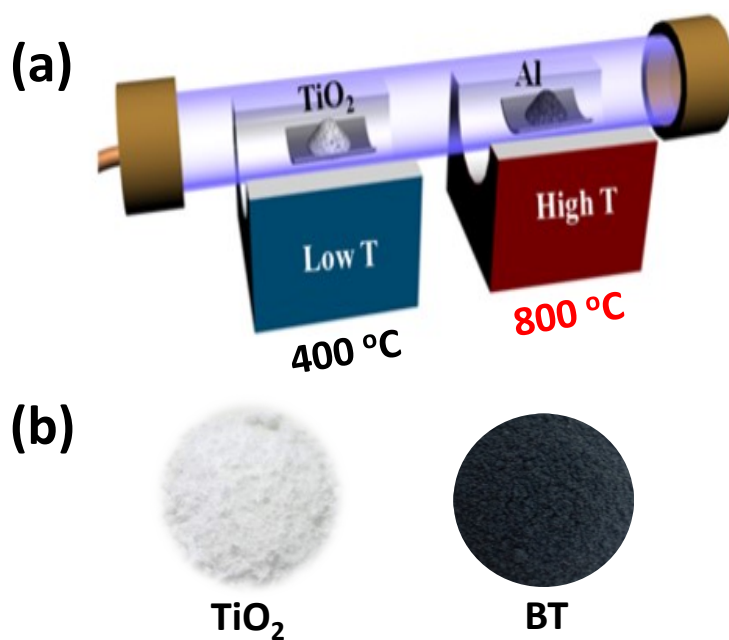
Fig. S1 (a) Schematic diagram of the two-zone tube furnace for BT's preparation via Al reduction, and (b) photographs of pristine TiO_2 and BT samples.
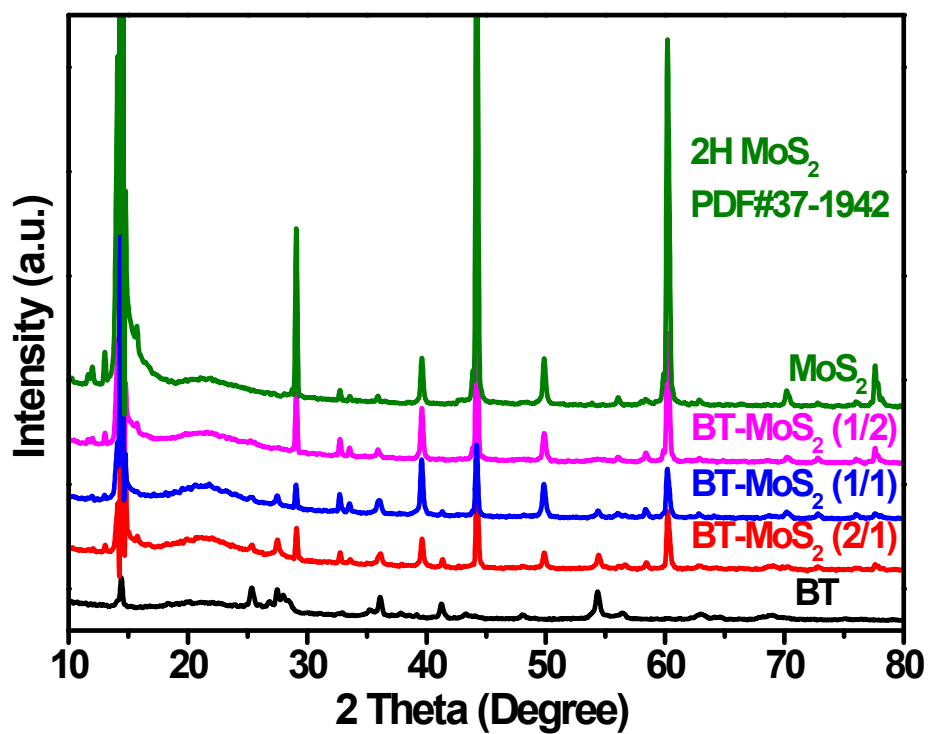

Fig. S2 XRD patterns of MoS_2, BT, and BT-MoS_2 samples.

Table S1. Characteristics of MoS$_2$, BT, and BT-MoS$_2$ samples.

Sample	BET surface area (m^2 g^{-1})	Pore volume (cm^3 g^{-1})	Pore diameter (nm)
BT	48.3	0.1789	17.1
MoS$_2$	31.5	0.0973	10.2
BT-MoS$_2$ (2/1)	45.9	0.1405	14.1
BT-MoS$_2$ (1/1)	50.2	0.1079	12.5
BT-MoS$_2$ (1/2)	46.7	0.1275	11.0
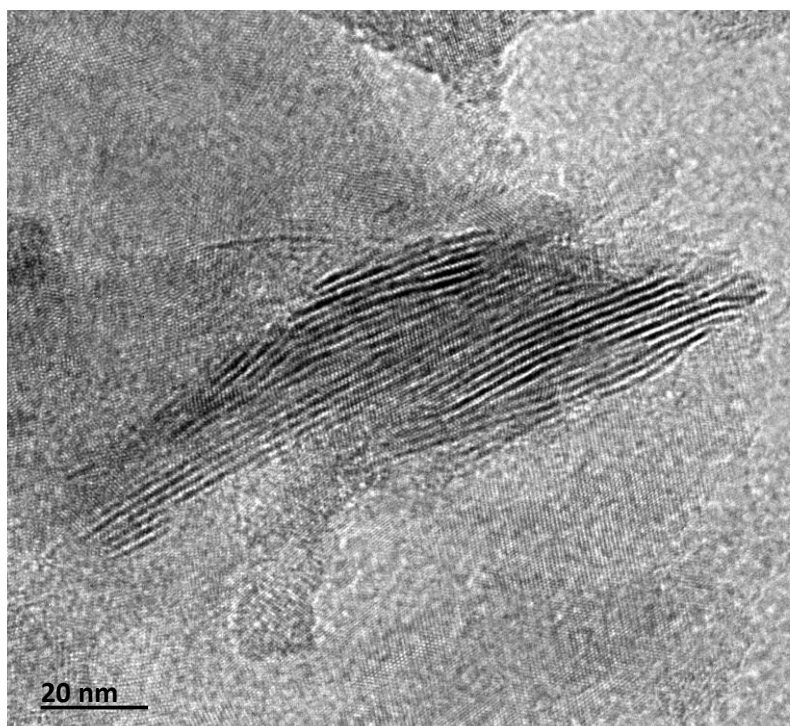
Fig. S3 TEM image of MoS$_2$ catalyst.
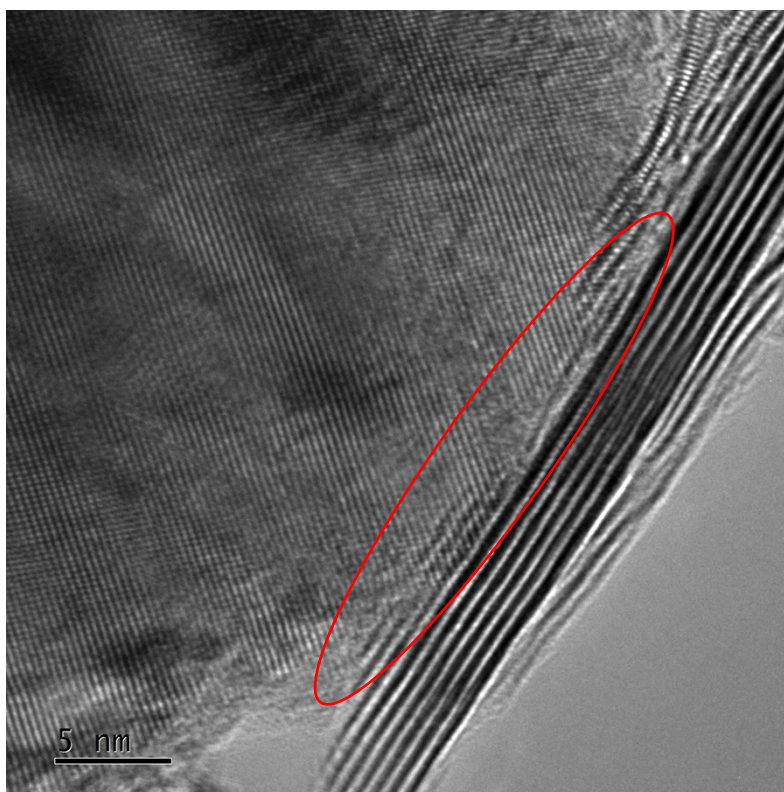
Fig. S4 HRTEM image of BT-MoS$_2$ (1/1) catalyst. Note that the junctions in the red circle indicate strong synergy between BT and MoS$_2$ components.
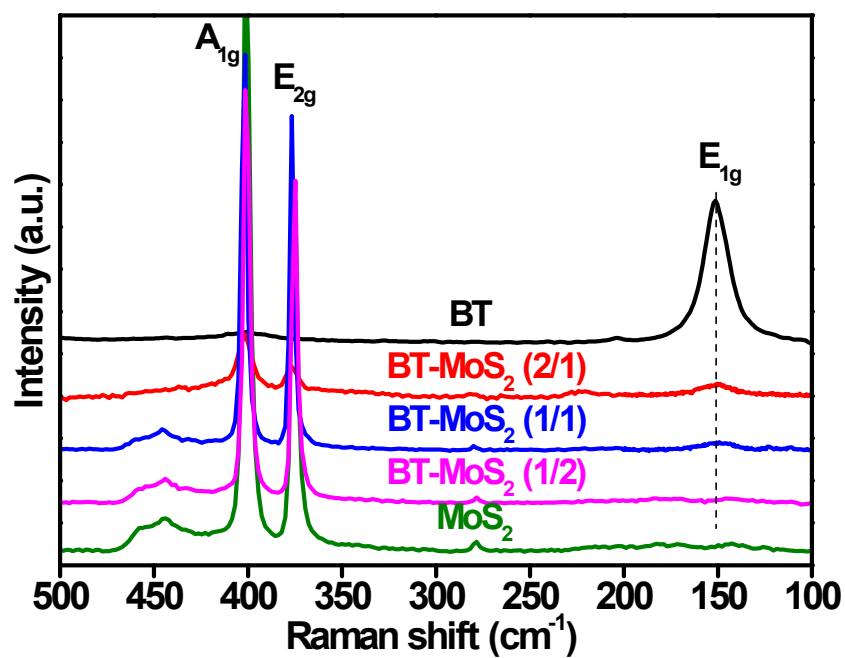
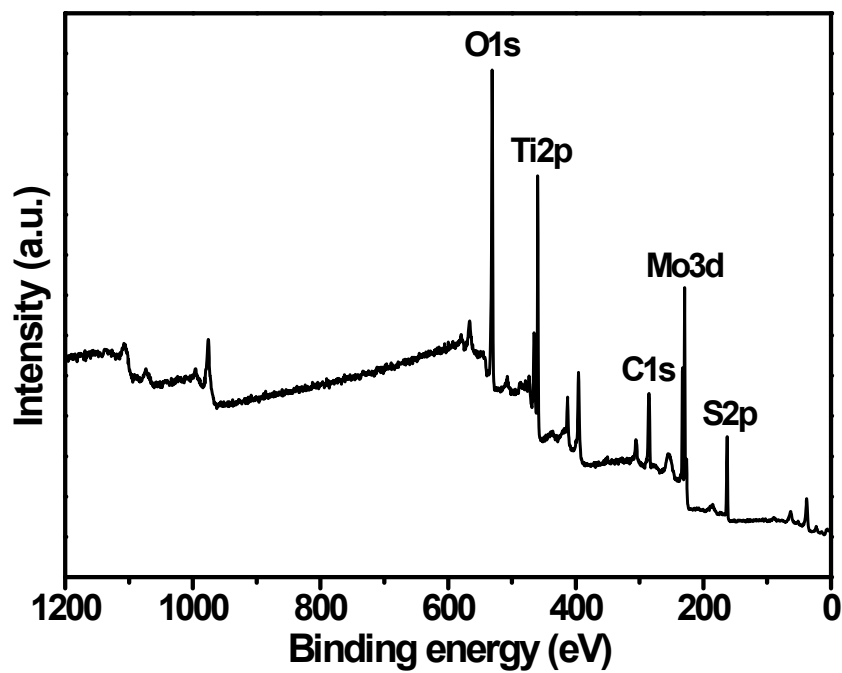**Fig. S5** Raman spectra of MoS$_2$, BT, and BT-MoS$_2$ samples.

Fig. S6 Full XPS spectrum of BT-MoS$_2$ (1/1) catalyst.

Table S2. The proportion of Ti^{3+}/Ti species of BT and BT-MoS$_2$ samples according to Ti2p$_{3/2}$ XPS data.

Sample	Ti^{3+}/Ti species[a]
BT	0.22
BT-MoS$_2$ (2/1)	0.18
BT-MoS$_2$ (1/1)	0.15
BT-MoS$_2$ (1/2)	0.11

[a] Calculated by the (peak area of Ti^{3+} species)/[(peak area of Ti^{3+} species) + (peak area of Ti^{4+} species)].
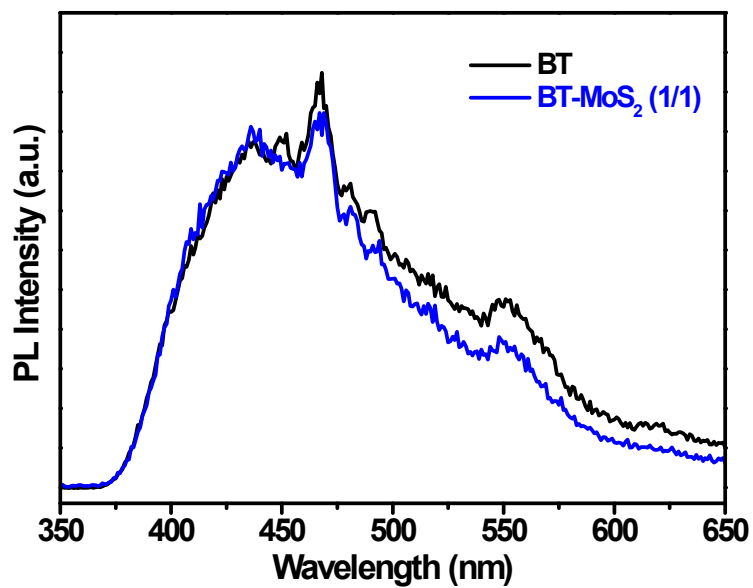
Fig. S7 PL spectra of BT and BT-MoS$_2$ (1/1) samples.
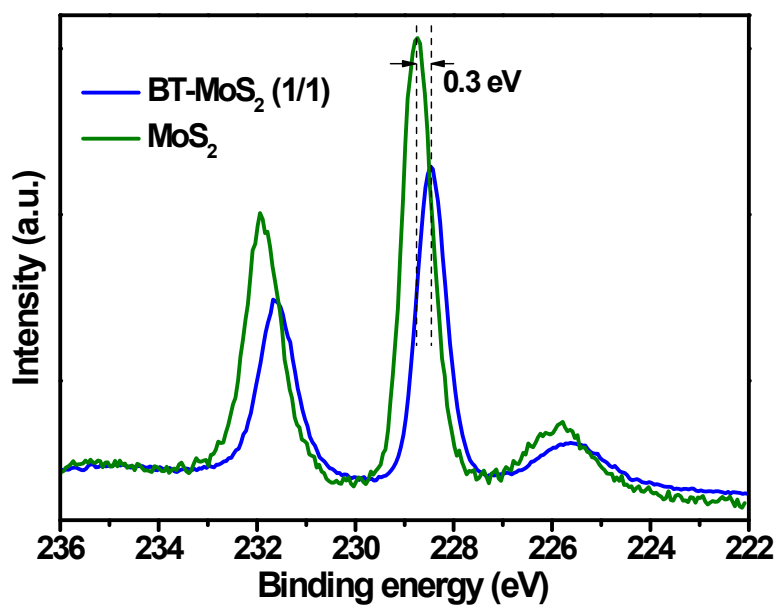
Fig. S8 XPS Mo3d spectra of MoS$_2$ and BT-MoS$_2$ (1/1) samples.
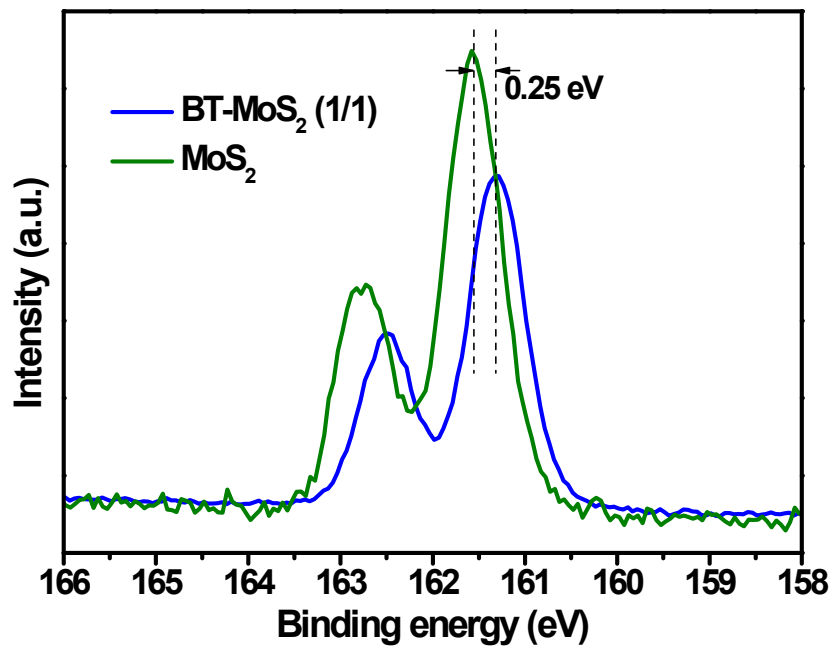
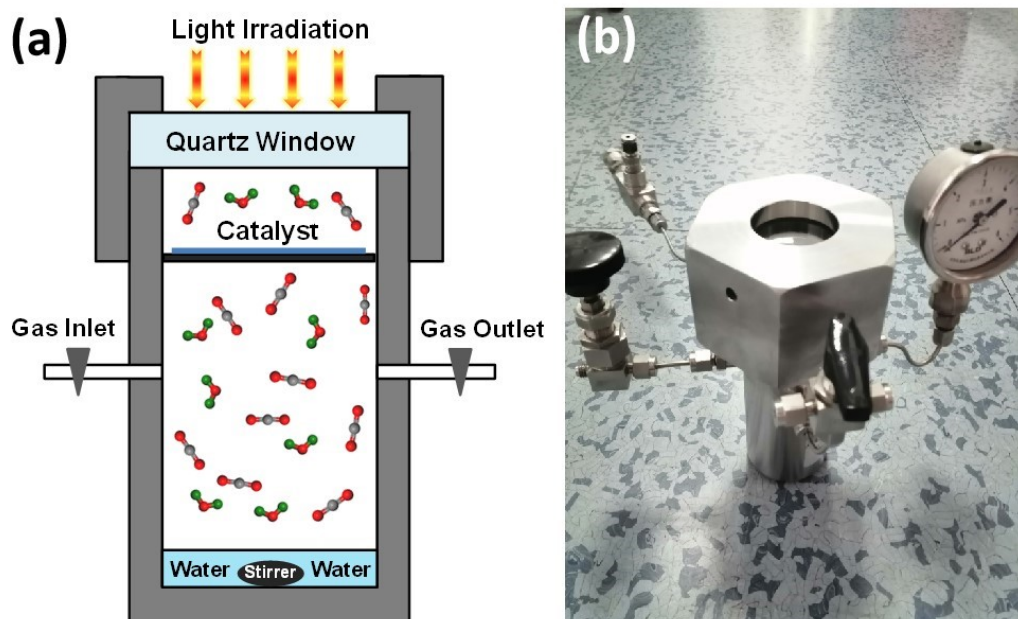**Fig. S9** XPS S2p spectra of MoS$_2$ and BT-MoS$_2$ (1/1) samples.

Fig. S10 (a) Schematic diagram and (b) actual object of the reactor for photocatalytic CO$_2$ reduction with moisture.

Table S3. Comparison of photocatalytic activity of CO_2 reduction over TiO_2-based catalysts.

| Catalyst	Reaction conditions	STY of CH_4 ($\mu mol\ g^{-1}\ h^{-1}$)	By-product	Reference
BP-BT	300 W Xe lamp, 2 bar, 6 mL H_2O	16.8	H_2, CO	S1
H-TiO_{2-x}	300 W Xe lamp, 2 bar, 6 mL H_2O	16.2	H_2, CO	S2
BT	300 W Xe lamp, 2 bar, 6 mL H_2O	14.3	H_2, CO	S3
P25	200 W Xe lamp, UV-Vis (λ = 320 ~ 780 nm), 2 bar	1.2	CO, H_2	S4
TiO_2 with {001} and {101} facets	300 W Xe lamp, ambient temperature, atmospheric pressure	1.35	—	S5
TiO_2 powder	75 W Hg lamp, λ > 280 nm	0.02	C_2H_4, C_2H_6	S6
Anatase particles	990 W Xe lamp, 0.96 KW m^{-2}, 90 bar	1.8	—	S7
Ti-PS (Si/Ti = 50, hexagonal)	100 W Hg lamp, UV irradiation, 323 K	7.1	CH_3OH	S8
Extracted TiO_2	UV 8 W Hg lamp, λ = 254 nm, supercritical fluid-grade CO_2	~ 4.3	—	S9
Ti-beta(OH)	100 W Hg lamp, λ > 250 nm	5.8	CH_3OH	S10
14 nm anatase particles	8 W Hg lamp, λ = 254 nm, supercritical fluid-grade CO_2	0.4	CH_3OH, H_2, CO	S11
P25 particles	15 W UV or near-UV lamp, λ = 365 or 254 nm, 316 K	4.11	CO, C_2H_6	S12
TiO_2 pellets	Three germicidal UVC lamps, λ = 253.7 nm	0.22 ($\mu mol\ h^{-1}$)	H_2, CO	S13
P25 particles	1000 W Xe lamp, λ < 700 nm, 343 K	0.1	H_2, CO	S14
Self-doped Ti^{3+}-rutile TiO_2	300 W Xe lamp, Vis-light, 1 atm	< 0.1	—	S15
Black TiO_2 films	Simulated sunlight, room temperature, continuous CO_2	12.0	CO	S16
Ti^{3+}-self doped brookite TiO_2	300 W Xe lamp, Vis-light, continuous CO_2	11.9	CO	S17
Reduced {001}-TiO_{2-x}	300 W Xe lamp, AM1.5	< 0.3	CO	S18
BT-MoS_2 (1/1)	300 W Xe lamp, simulated solar, 2 bar	18.1	H_2, CO	this work
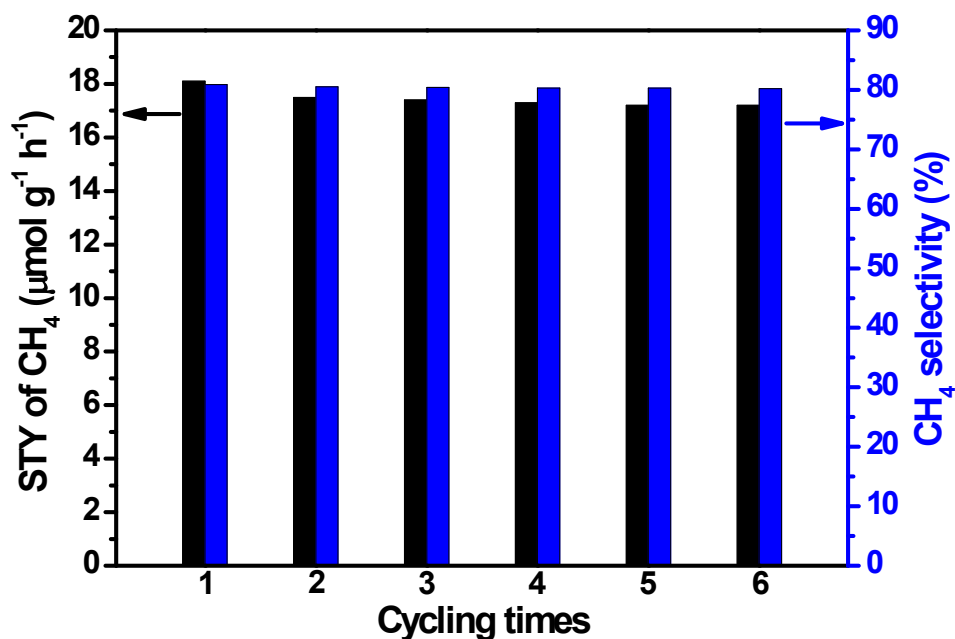
Fig. S11 Recycling of BT-MoS$_2$ (1/1) catalyst for photocatalytic CO$_2$ reduction to CH$_4$ under solar light irradiation. Reaction conditions: 50 mg catalyst, 2 bar CO$_2$, 6 mL H$_2$O, 5 h in each run.

Table S4. The CH$_4$ generation rate of photocatalytic CO$_2$ reduction over TiO$_2$, BT, and BT-MoS$_2$ (1/1) samples.[a]

Catalyst	Substrate	STY[b] of CH$_4$
TiO$_2$	H$_2$O/CO$_2$	1.8
TiO$_2$	D$_2$O/CO$_2$	1.2
TiO$_2$	H$_2$O/^{13}CO$_2$	1.0
TiO$_2$	D$_2$O/^{13}CO$_2$	0.6
BT	H$_2$O/CO$_2$	14.3
BT	D$_2$O/CO$_2$	10.2
BT	H$_2$O/^{13}CO$_2$	8.4
BT	D$_2$O/^{13}CO$_2$	5.6
BT-MoS$_2$ (1/1)	H$_2$O/CO$_2$	18.1
BT-MoS$_2$ (1/1)	D$_2$O/CO$_2$	13.9
BT-MoS$_2$ (1/1)	H$_2$O/^{13}CO$_2$	11.3
BT-MoS$_2$ (1/1)	D$_2$O/^{13}CO$_2$	7.5

[a] Reaction conditions: 50 mg catalyst, 2 bar CO$_2$, 6 mL H$_2$O, solar light for 5 h.

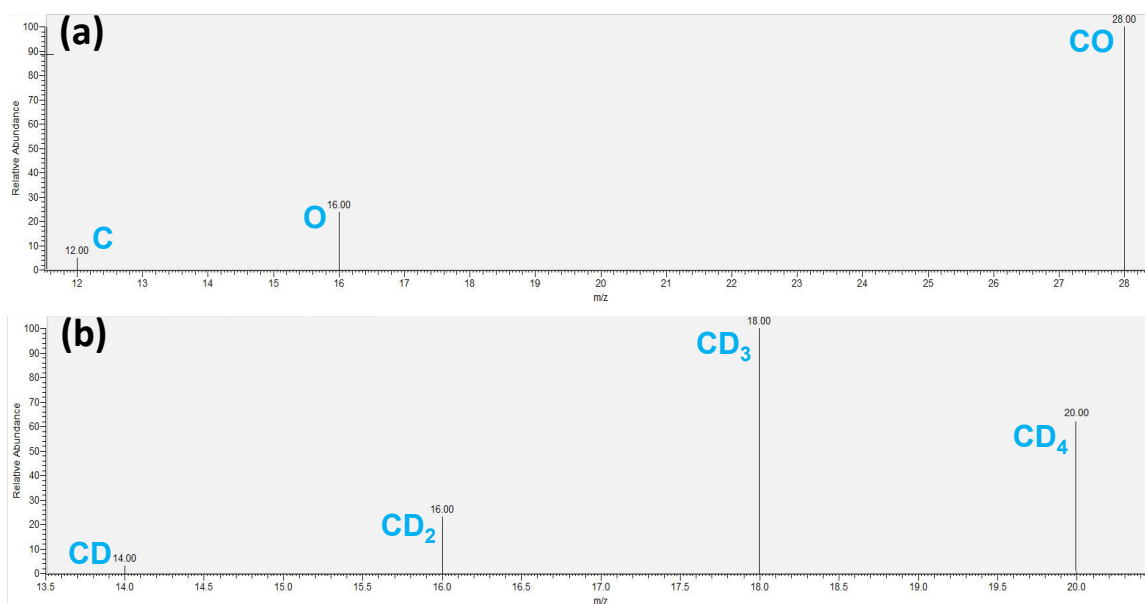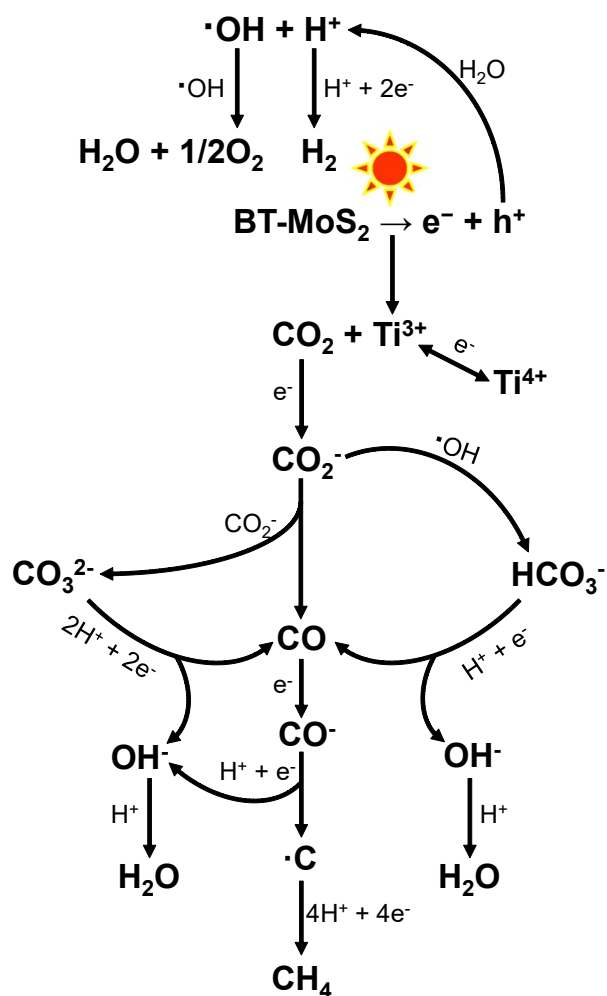[b] The unit of STY is μmol g^{-1} h^{-1}.

Fig. S12 GC-MS data of (a) CO and (b) CD_4 generated over $BT-MoS_2$ (1/1) sample photocatalyzed D_2O/CO_2 transformation under solar light irradiation.

Scheme S1 Proposed reaction mechanism of the photocatalytic CO_2 reduction over $BT-MoS_2$ catalyst.
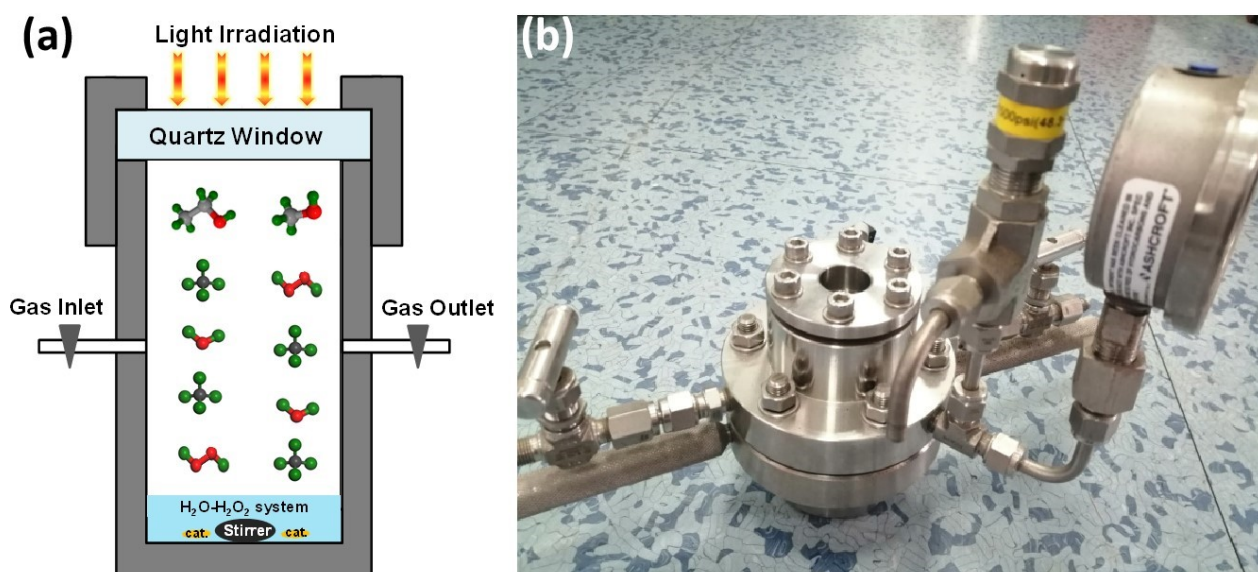
Fig. S13 (a) Schematic diagram and (b) actual object of the reactor for H_2O_2-assisted photocatalytic CH_4 transformation.
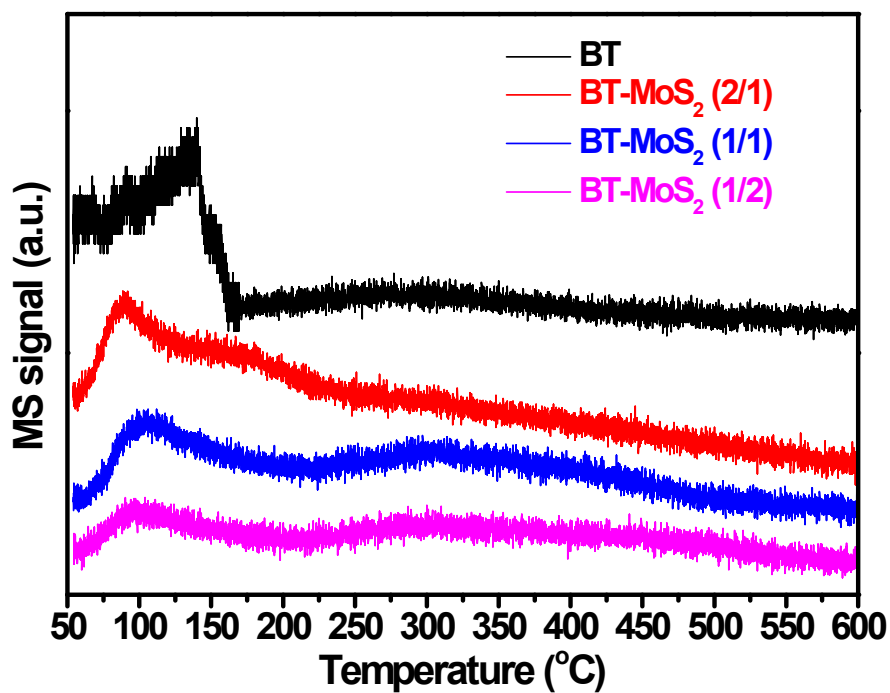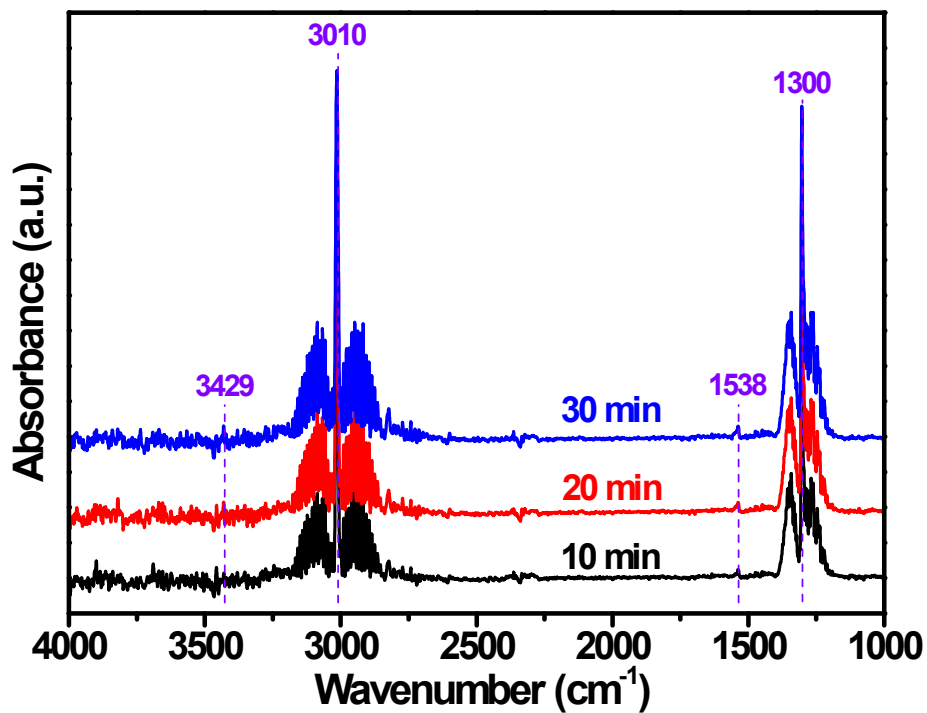

Fig. S14 CH_4-TPD profiles of BT and BT-MoS_2 samples.

Fig. S15 *In situ* DRIFT spectra of CH$_4$-H$_2$O$_2$ adsorption on BT-MoS$_2$ (1/1) sample. Note that the peaks at 1300 and 1538 cm^{-1} are attributed to the C−H deformation vibration of CH$_4$ and C−H symmetric deformation vibrational mode of CH$_4$,[S19] respectively. The peaks at 3010 and 3429 cm^{-1} are ascribed to the OH species.[S19]
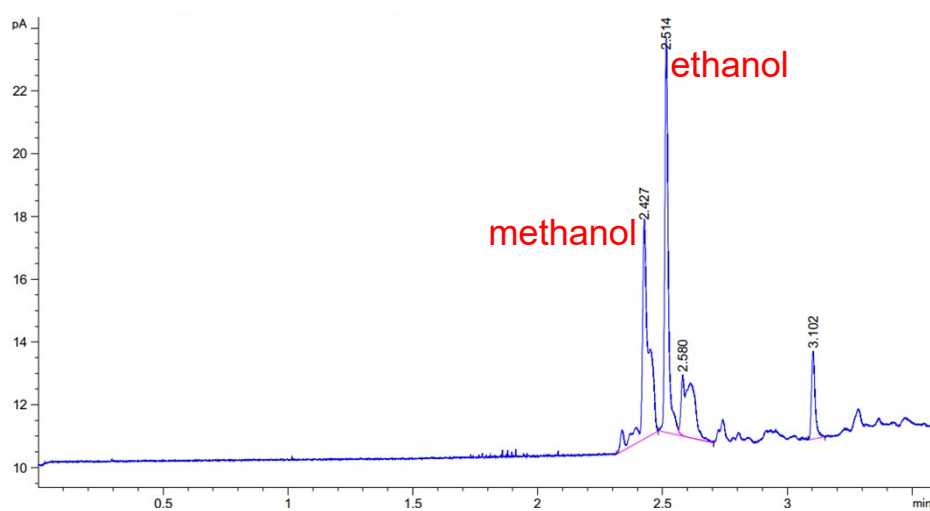

Fig. S16 GC-FID data of solar-light-driven photocatalytic CH$_4$ oxidation to alcohols over BT-MoS$_2$ (1/1).
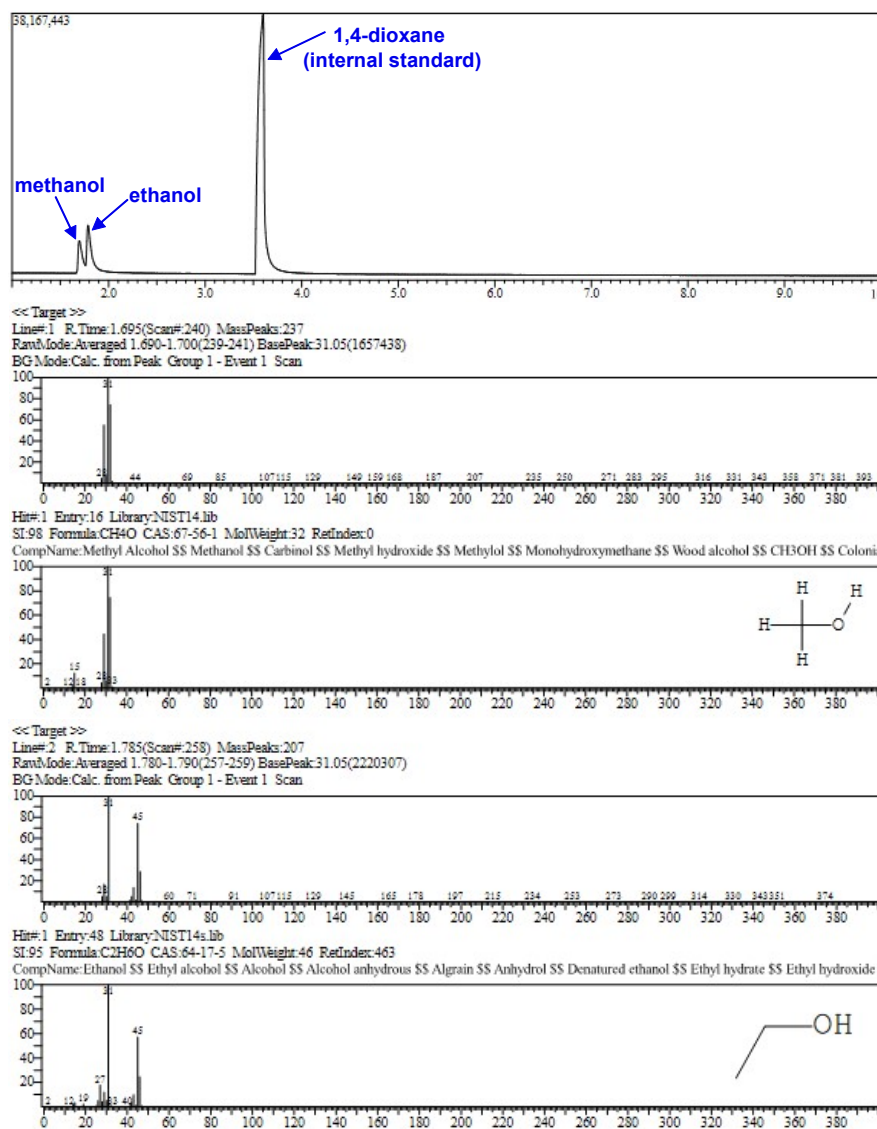
Fig. S17 GC-MS data of solar-light-driven photocatalytic CH_4 oxidation to alcohols over BT-MoS$_2$ (1/1).

Table S5. Comparison of photocatalytic activity of CH_4 oxidation to alcohols over solid catalysts.

Catalyst	Reaction conditions	STY of methanol (μmol g^{-1} h^{-1})	STY of ethanol (μmol g^{-1} h^{-1})	alcohol sel. (%)	Ref.
Ag$_2$O@WO$_3$	100 mJ and 355 nm laser beam, 100 mL min^{-1} CH$_4$, 70 mL H$_2$O	600	0	—	S20
BiVO$_4$	350 W Xe lamp, 10% CH$_4$/Ar with bubbler, 20 mL H$_2$O, 65 °C	134	0	85	S21
FeO$_x$/TiO$_2$	300 W Xe lamp, 70 μmol CH$_4$, 8 μmol H$_2$O$_2$ in 10 mL H$_2$O	352	26.5	97	S22

|				
Cu-0.5/PCN	500 W Xe lamp, 10 mL min^{-1} CH$_4$, 90 mL min^{-1} N$_2$, 25 mL H$_2$O	24.5	106	81.2	S23
g-C$_3$N$_4$@Cs$_{0.33}$WO$_3$	300 W Xe lamp, 1000 ppm CH$_4$ in air	4.38	0	51.6	S24
Au-CoO$_x$/TiO$_2$	300 W Xe lamp, 0.1 MPa O$_2$ and 2 MPa CH$_4$, 100 mL H$_2$O	2540 for CH$_3$OH and CH$_3$OOH	0	95	S19
Fe^{3+}-WO$_3$/KIT-6	mercury-vapor lamp, 4.5 mL min^{-1} CH$_4$, 17.9 mL min^{-1} He, 300 mL H$_2$O, 55 ^{o}C	67.5	0	58.5	S25
WO$_3$/La	mercury-vapor lamp, 4.5 mL min^{-1} CH$_4$, 17.9 mL min^{-1} He, 300 mL H$_2$O, 55 ^{o}C	31.3	0	47	S26
CeO$_2$-1100	300 W Xe lamp, 4 mL min^{-1} CH$_4$, 15 mL H$_2$O	0	11.4	91.5	S27
RCN-5	300 W Xe lamp, 0.1 MPa O$_2$ and 2 MPa CH$_4$, 20 mL H$_2$O	30	281.6	82	S28
TiO$_2$	300 W Xe lamp, 3 MPa CH$_4$, 2 mL 0.01 M FeCl$_2$, 200 μL H$_2$O$_2$, 20 mL H$_2$O	471	0	83	S29
Au/ZnO	300 W Xe lamp, 0.1 MPa O$_2$ and 2 MPa CH$_4$, 100 mL H$_2$O	2060	0	15.6	S30
Au/ZnO	300 W Xe lamp, 5 bar O$_2$ and 15 bar CH$_4$, 10 mL H$_2$O	685	0	99.1	S31
FeOOH/m-WO$_3$	300 W Xe lamp, visible light source, 10 mL min^{-1} CH$_4$, 90 mL min^{-1} N$_2$, 2 mL H$_2$O$_2$, 18 mL H$_2$O	211.2	0	91	S32
BT-MoS$_2$ (1/1)	300 W Xe lamp, 20 bar CH$_4$, 1 mL 30% H$_2$O$_2$ and 9 mL H$_2$O	52.6	68.5	95.6	this work
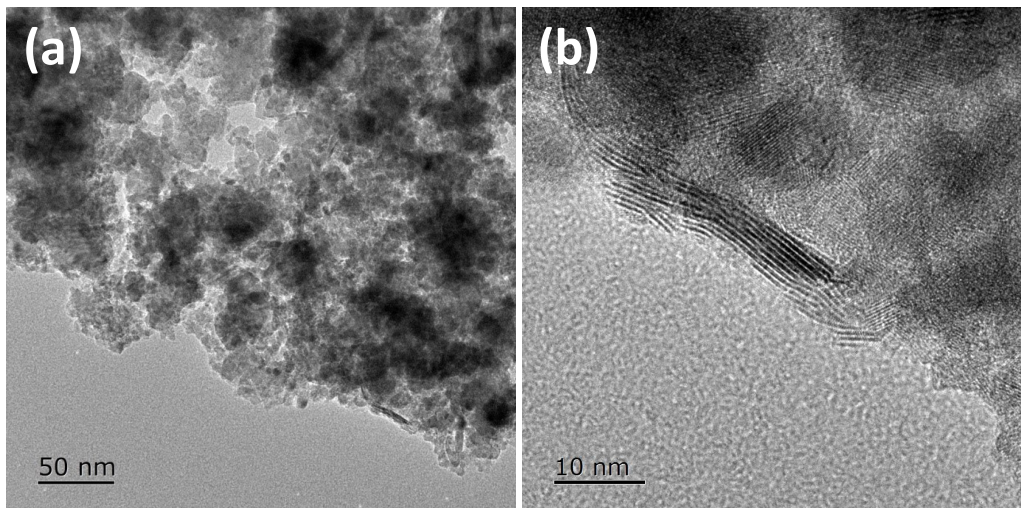
Fig. S18 HRTEM images of the used BT-MoS$_2$ (1/1) catalyst.
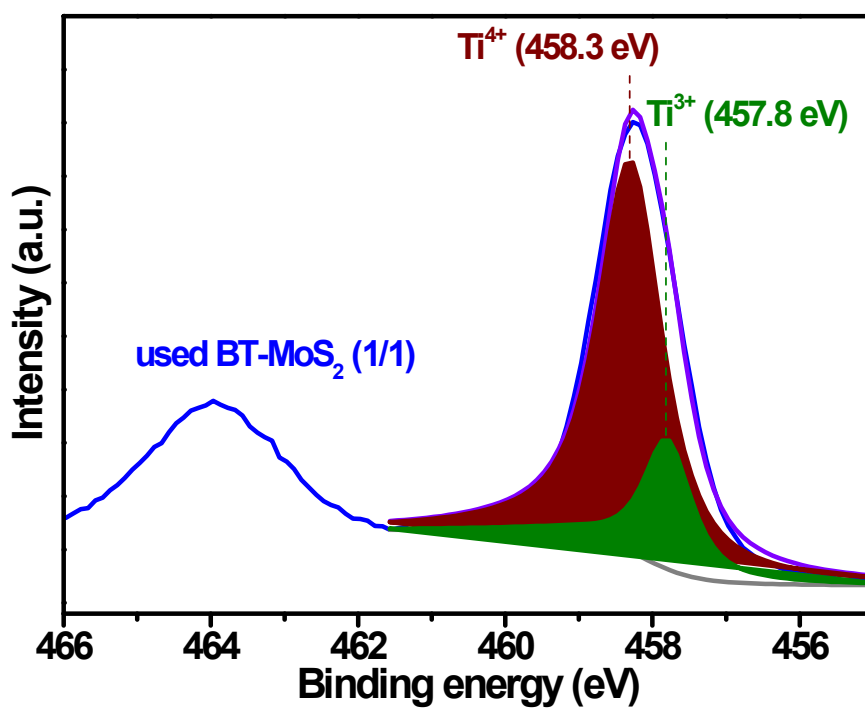

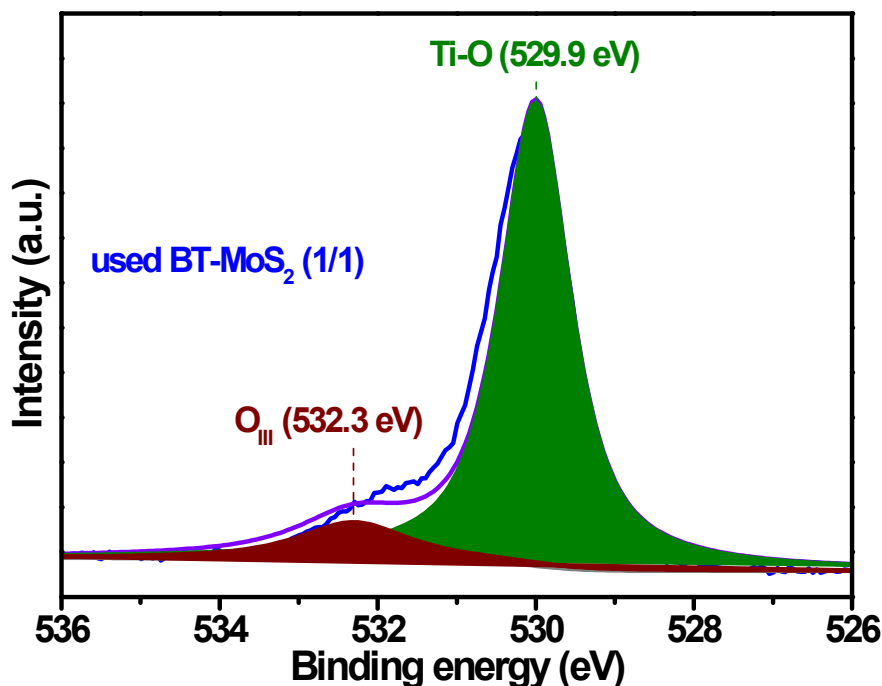**Fig. S19** XPS Ti2p spectrum of the used BT-MoS$_2$ (1/1) catalyst.

Fig. S20 XPS O1s spectrum of the used BT-MoS$_2$ (1/1) catalyst.

Supplementary References:

(S1) Q. Bi, K. Hu, J. Chen, Y. Zhang, M. S. Riaz, J. Xu, Y. Han, F. Huang, *Appl. Catal. B* 2021, **295**, 120211.

(S2) G. Yin, X. Huang, T. Chen, W. Zhao, Q. Bi, J. Xu, Y. Han, F. Huang, *ACS Catal.* 2018, **8**, 1009.

(S3) G. Yin, Q. Bi, W. Zhao, J. Xu, T. Lin, F. Huang, *ChemCatChem* 2017, **9**, 4389.

(S4) Q. Zhai, S. Xie, W. Fan, Q. Zhang, Y. Wang, W. Deng, Y. Wang, *Angew. Chem. Int. Ed.* 2013, **52**, 5776.

(S5) J. Yu, J. Low, W. Xiao, P. Zhou, M. Jaroniec, *J. Am. Chem. Soc.* 2014, **136**, 8839.

(S6) M. Anpo, H. Yamashita, Y. Ichihashi, S. Ehara, *J. Electroanal. Chem.* 1995, **396**, 21.

(S7) S. Kaneco, H. Kurimoto, Y. Shimizu, K. Ohta, T. Mizuno, *Energy* 1999, **24**, 21.

(S8) K. Ikeue, S. Nozaki, M. Ogawa, M. Anpo, *Catal. Today* 2002, **74**, 241.

(S9) K. Koci, L. Matejova, L. Obalova, L. Capek, J. C. S. Wu, *J. Sol-Gel Sci. Techn.* 2015, **3**, 621.

(S10) K. Ikeue, H. Yamashita, M. Anpo, T. Takewaki, *J. Phys. Chem. B* 2001, **105**, 8350.

(S11) K. Koci, L. Obalova, L. Matejova, D. Placha, Z. Lacny, J. Jirkovsky, O. Solcova, *Appl. Catal. B* 2009, **89**, 494.

(S12) C. C. Lo, C. H. Hung, C. S. Yuan, J. F. Wu, *Sol. Energy Mater. Sol. Cells* 2007, **91**, 1765.

(S13) S. S. Tan, L. Zou, E. Hu, *Sci. Technol. Adv. Mater.* 2007, **8**, 89.

(S14) F. Saladin, L. Forss, I. Kamber, *J. Chem. Soc. Chem. Commun.* 1995, 533.

(S15) K. Sasan, F. Zuo, Y. Wang, P. Feng, *Nanoscale* 2015, **7**, 13369.

(S16) Q. Wang, Z. Zhang, X. Cheng, Z. Huang, P. Dong, Y. Chen, X. Zhang, *J. CO$_2$ Util.* 2015, **12**, 7.

(S17) X. Xin, T. Xu, L. Wang, C. Wang, *Sci. Rep.* 2016, **6**, 23684.

(S18) W. Fang, L. Khrouz, Y. Zhou, B. Shen, C. Dong, M. Xing, S. Mishra, S. Daniele, J. Zhang, *Phys. Chem. Chem. Phys.* 2017, **19**, 13875.

(S19) H. Song, X. Meng, S. Wang, W. Zhou, S. Song, T. Kako, J. Ye, *ACS Catal.* 2020, **10**, 14318.

(S20) A. Hameed, I. M. I. Ismail, M. Aslam, M. A. Gondal, *Appl. Catal. A* 2014, **470**, 327.

(S21) W. Zhu, M. Shen, G. Fan, A. Yang, J. R. Meyer, Y. Ou, B. Yin, J. Fortner, M. Foston, Z. Li, Z. Zou, B. Sadtler, *ACS Appl. Nano Mater.* 2018, **1**, 6683.

(S22) J. Xie, R. Jin, A. Li, Y. Bi, Q. Ruan, Y. Deng, Y. Zhang, S. Yao, G. Sankar, D. Ma, J. Tang, *Nat. Catal.* 2018, **1**, 889.

(S23) Y. Zhou, L. Zhang, W. Wang, *Nat. Commun.* 2019, **10**, 506.

(S24) Y. Li, J. Li, G. Zhang, K. Wang, X. Wu, *ACS Sustainable Chem. Eng.* 2019, **7**, 4382.

(S25) K. Villa, S. Murcia-López, T. Andreu, J. R. Morante, *Appl. Catal. B* 2015, **163**, 150.

(S26) K. Villa, S. Murcia-López, J. R. Morante, T. Andreu, *Appl. Catal. B* 2016, **187**, 30.

(S27) J. Du, W. Chen, G. Wu, Y. Song, X. Dong, G. Li, J. Fang, W. Wei, Y. Sun, *Catalysts* 2020, **10**, 196.

(S28) Z. Yang, Q. Zhang, L. Ren, X. Chen, D. Wang, L. Liu, J. Ye, *Chem. Commun.* 2021, **57**, 871.

(S29) Y. Zeng, H. C. Liu, J. S. Wang, X. Y. Wu, S. L. Wang, *Catal. Sci. Technol.* 2020, **10**, 2329.

(S30) H. Song, X. Meng, S. Wang, W. Zhou, X. Wang, T. Kako, J. Ye, *J. Am. Chem. Soc.* 2019, **141**, 20507.

(S31) W. Zhou, X. Qiu, Y. Jiang, Y. Fan, S. Wei, D. Han, L. Niu, Z. Tang, *J. Mater. Chem. A* 2020, **8**, 13277.

(S32) J. Yang, J. Hao, J. Wei, J. Dai, Y. Li, *Fuel* 2020, **266**, 117104.